Journal of Materials and Environmental Sciences
ISSN : 2028-2508

JMES, 2017 Volume 8, Issue 5, Page 1860-1876

http://www.jmaterenvironsci.com

A DFT and Molecular Dynamics Study on Inhibitory Action of indazole Derivative on Corrosion of Mild Steel

M. M. Mohamed Abdelahi[1], H. Elmsellem[2*], M. Benchidmi[1], N. K. Sebbar[1], M.A. Belghiti[2], L. El Ouasif[1], A. E. Jilalat[1], Y. Kadmi[4,5,6,7], E. M. Essassi[1,3]

[1]*Laboratoire de Chimie Organique Hétérocyclique, URAC 21, Pôle de Compétences Pharmacochimie, Mohammed V University in Rabat, Faculté des Sciences, Av. Ibn Battouta, BP 1014 Rabat, Morocco.*
[2]*Laboratoire de chimie analytique appliquée, matériaux et environnement (LC2AME), Faculté des Sciences, B.P. 717, 60000 Oujda, Morocco.*
[3]*Moroccan Foundation for Advanced Science, Innovation and Research (MASCIR), Rabat Design Center, Rue Mohamed Al Jazouli, Madinat El Irfane, Rabat, Morocco.*
[4]*Université d'Artois, EA 7394, Institut Charles Viollette, Lens, F-62300, France*
[5]*ISA Lille, EA 7394, Institut Charles Viollette, Lille, F-59000, France*
[6]*Ulco, EA 7394, Institut Charles Viollette, Boulogne sur Mer, F-62200, France*
[7]*Université de Lille, EA 7394, Institut Charles Viollette, Lille, F-59000, France*

Received 25 Dec 2016,
Revised 31 Jan 2017,
Accepted 04 Feb 2017

Keywords
- ✓ Indazole*;*
- ✓ EIS *;*
- ✓ Corrosion*;*
- ✓ Electrochemical*;*
- ✓ DFT*;*
- ✓ Fukui function *;*
- ✓ Monte Carlo *;*

H. Elmsellem
h.elmsellem@gmail.com
Phone: (+212)0670923431

Abstract

The corrosion inhibition performance of indazole derivative namely 1-benzyl-6-nitro-1H-indazole (P1) on mild steel corrosion in 1M HCl has been studied using gravimetric, electrochemical impedance spectroscopy (EIS), Potentiodynamic polarization, scanning electron microscopy (SEM), DFT and Monte Carlo simulation. The corrosion inhibition efficiency at optimum concentration (10^{-3}M) is 91% (P1). P1 obeyed Langmuir adsorption isotherm. SEM analyses supported formation of protective film on mild steel in presence of inhibitor. DFT and Monte Carlo simulation calculations supported experimental results.

1. Introduction

The corrosion phenomenon of materials [1] is an important topic in many industries because of its consequences on industrial equipment including vessels, engineering vehicles, mining equipment, packaging machineries, etc. Corrosion mostly involves the deterioration of the materials and it is widely common in metals. The use of inhibitors [2] is one of the most practical methods to protect metals against corrosion, especially in acidic media. Most of the organic inhibitors [3, 4] containing nitrogen, oxygen, sulphur, phosphorus atoms, and multiple bonds in their molecules facilitate adsorption on the metal surface. Many researchers [5] conclude that the adsorption on the metal surface depends mainly on the physicochemical properties of the inhibitor, such as the functional group, molecular electronic structure, electron density at the donor atom, π orbital character and the molecular size. The planarity and the lone electron pairs in the heteroatoms [6] are important features that determine the adsorption of molecules on the metallic surface.

A large number of organic compounds [7-9] have been investigated as corrosion inhibitors for different types of metals. With increased awareness towards environmental pollution and control, the search for less toxic and

environmentally friendly corrosion inhibitors is becoming increasingly important. Thus, researchers focused their works on several drugs, including molecules in the class of β-lactam antibiotics [10, 11], cephalosporins [12], quinolones [13-15], antifungal drugs [16], etc.

Quantum chemical calculations have been widely used to study reactive mechanism and to elucidate many experimental observations. They have been proved [17, 18] to be a very powerful tool for studying corrosion inhibition mechanism. Density functional theory (DFT) [19, 20] has provided a very useful framework for developing new criteria for rationalizing, predicting and eventually understanding many aspects of chemical processes [21, 22]. During the last decades, density functional theory has undergone fast development, especially in the field of organic chemistry, as the number of accurate exchange-correlation functionals increased. Moreover, starting from the work of Fukui and its frontier molecular orbitals (FMOs) theory [27], the same authors further generalized the concept and proposed the Fukui function as a tool for describing the local reactivity in molecules [28].

The 1H-indazole nucleus is rarely found in nature [29-31] and their derivatives have a considerable importance in pharmaceutical industry. [32-34] . With respect to biological applications, these derivatives are found potent (anticancer, antimicrobial, and other important therapeutic properties) [35-36]. Before moving on to synthetic methods, the Studies of the structure and physicochemical properties of indazole ring have been reviewed by Speranza M., et al [37]. The lack of methods to prepare indazole has recently inspired several groups to develop routes to these compounds [38-41]. Additionally, the nitro-indazole, and its derivatives have received much attention, as their intriguing physical and biological properties including, leishmanicidal activity, anti-inflammatory, anti-viral, anti-microbial, anti-cancer, anti-platelet and anti-spermatogenic activity [42].

In this work, the efficacy of the organic compound 1-benzyl-6-nitro-1*H*-indazole (**Fig 1**) as an acid corrosion inhibitor for copper in nitric acid solution, using mass loss technique and to analyze the inhibition efficiency in the light of the global and local quantum chemical parameters.

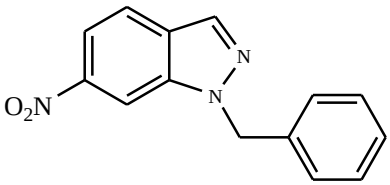

Figure 1. Chemical structure of 1-benzyl-6-nitro-1*H*-indazole (P1).

2. Experimental

2.1. Synthesis of inhibitor

To a solution of 6-nitro-1H-indazole (1 g, 5 mmol) in THF (30 ml) were added benzyl bromide (0.8 g, 5 mmol), potassium carbonate (0,9 g, 4 mmol) and a catalytic quantity of tetra-n-butylammonium iodide. The mixture was stirred at room temperature for 48 h. The solution was filtered and the solvent removed under reduced pressure. The residue was recrystallized from ethanol to afford the title compound as yellow powder (yield: 70%).

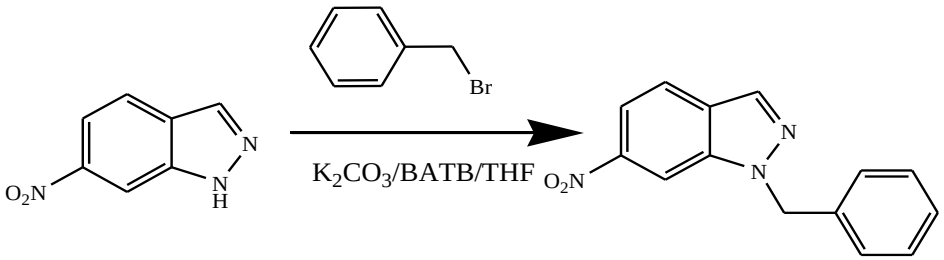

Scheme 1. Synthesis of 1-benzyl-6-nitro-1*H*-indazole (P1).

Yield:63%; **mp:** 391**K** ; **^{1}H NMR ($CDCl_3$; 300MHz) δ (ppm) :** 5.83 (s, 2H, NCH2), 7.22-7.29 (m, 5H, CHAr), 7,9 (dd, J = 9HZ; J=1,9HZ, 1H, H5), 8,01 (dd, J = 9HZ; J= 0,6HZ,H4).8.35 (d, J= 0,9HZ, 1H H3), 8,8.(d, J= 1,9HZ, 1H,H7).**^{13}C NMR ($CDCl_3$;75MHz) δ(ppm)**: 52.5 (NCH2), 107.3-115.5-122.8-127.9-128-129.9 (6CHAr),134.5 (CH=N), 127.2-134.5- 138.5-146.5 (Cq).

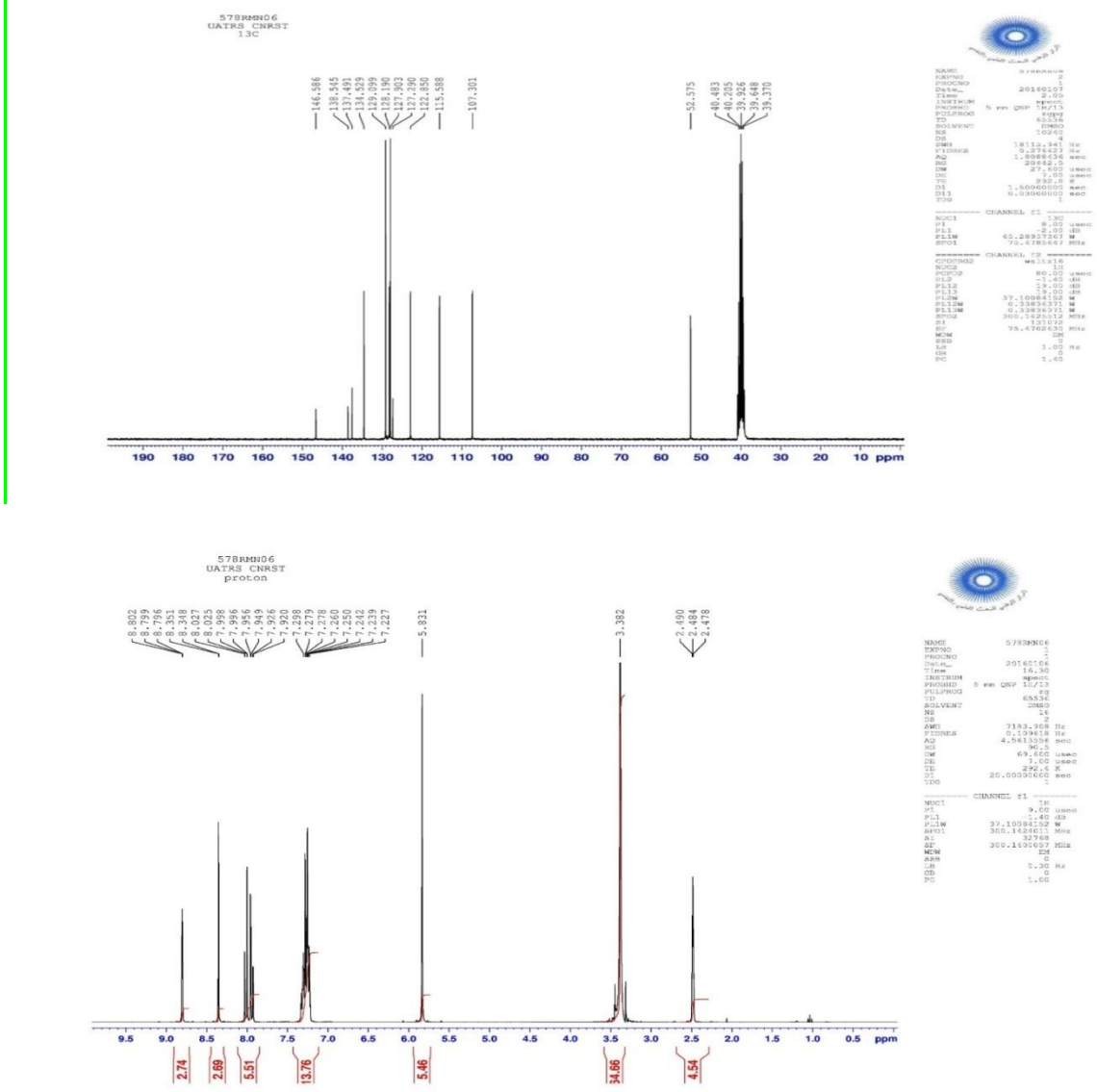

Figure 2: ^{1}H NMR and ^{13}C NMR spectrum of P1.

2.2. Experimental procedure

For the weight loss technique the investigated steel materials of chemical composition in weight (0.2% C, 0.38% Si, 0.09% P, 0.01% Al, 0.05% Mn, 0.05% S). The samples of mild steel were mechanically polished with different emery paper SiC (grade 120, 1200) before each experiment, washed with distilled water and acetone and finally dried at room temperature.

The aggressive solution 1 M HCl is prepared by dilution of Analytical Grade 37% HCl with bidistilled water and the concentration range of inhibitors was 10^{-3}–10^{-6}M. Gravimetric measurements were carried out in a double walled glass cell equipped with a thermostat-cooling condenser, before immersion. The initial weight of each specimen was noted using an analytical balance and then the specimens were immersed in HCl solutions with and without inhibitor after 6 h of immersion at 308K the specimens were washed and reweighed. Electrochemical measurements were conducted using a potentiostat PGZ100 piloted by Voltamaster software and connected to a conventional three electrode cylindrical Pyrex glass cell. The working electrode (WE) had the form of a disc cut from the steel sheet, a saturated calomel electrode (SCE) was used as reference and a platinum plate was used as counter electrode. Before all experiments, the potential was stabilized at free potential during 30 min, the polarization measurements were performed by applying a controlled potential scan automatically from –800 to –200 mV at a scan rate of 1 mV/s [43]. A 10 mV peak to- peak sine wave over an

frequency range extending from 10 mHz to 100 MHz was used for the impedance measurements. All tests have been performed in non-deaerated solutions and the impedance diagrams are given in the Nyquist and Bod representation. All electrochemical studies were made at 308 K for an immersion time of 1/2 h, with different concentrations of inhibitor.

2.3. Quantum Chemical Calculations

All the quantum chemical calculations have been carried out with Gaussian 09 programme package [44-45]. In our calculation we have used B3LYP, a hybrid functional of the DFT method, which consists of the Becke's three parameters; exact exchange functional B3 combined with the nonlocal gradient corrected correlation functional of Lee-Yang-Par (LYP) has been used along with 6-31G(d, p) basis set. In the process of geometry optimisation for the fully relaxed method, convergence of all the calculations has been conirmed by the absence of imaginary frequencies. The aim of our calculation is to calculate the following quantum chemical indices: the energy of highest occupied molecular orbital (E_{HOMO}), the energy of lowest unoccupied molecular orbital (E_{LUMO}), energy gap (ΔE), hardness (η), sotness (σ), electrophilicity index (ω), the fraction of electrons transferred (ΔN) from inhibitor molecule to the metal surface, and energy change when both processes occur, namely, and correlate these with the experimental observations.
The electronic populations as well as the Fukui indices and local nucleophilicities are computed using NPA (natural population analysis) [46–48]. Our objective, in this study, is to investigate computationally inhibitory action of isatin derivative **E1** with chloridric acid in gas and in aqueous phase using B3LYP method with 6-31G(d, p) basis set.

2.3.1. Theory and computational details

Theoretical study of bezothiazine derivative with chloridric acid as corrosion inhibitors was done by using the Density Functional Theory (DFT) with the B3LYP [49] /6-31G(d, p) method implemented in Gaussian 09 program package.
In this study, some molecular properties were calculated such as the frontier molecular orbital (HOMO and LUMO) energies, energy gap (E_{Gap}), charge distribution, electron affinity (A), ionization
Popular qualitative chemical concepts such as electronegativity [50, 51] (χ) and hardness [52] (η) have been provided with rigorous definitions within the purview of conceptual density functional theory [53–55].
Using a finite difference method, working equations for the calculation of χ and η may be given as [53]:

$$\chi = \frac{I+A}{2} \quad \text{or} \quad \chi = -\frac{E_{HOMO}+E_{LUMO}}{2} \qquad (1)$$

$$\eta = \frac{I-A}{2} \quad \text{or} \quad \eta = -\frac{E_{HOMO}-E_{LUMO}}{2} \qquad (2)$$

Where $I = -E_{HOMO}$ and $A = -E_{LUMO}$ are the ionization potential and electron affinity respectively.
Local quantities such as Fukui function defined the reactivity/selectivity of a specific site in a molecule.
Using left and right derivatives with respect to the number of electrons, electrophilic and nucleophilic Fukui functions for a site k in a molecule can be defined [56].

$$f_k^+ = q_k(N+1) - q_k(N) \quad for\ nucleophilic\ attack \qquad (3)$$

$$f_k^- = q_k(N) - q_k(N-1) \quad for\ electrphilic\ attack \qquad (4)$$

$$f_k^+ = [q_k(N+1) - q_k(N-1)]/2 \quad for\ radical\ attack \qquad (5)$$

where, $q_k(N)$, $q_k(N+1)$ and $q_k(N-1)$ are the natural populations for the atom k in the neutral, anionic and cationic species respectively.
The fraction of transferred electrons ΔN was calculated according to Pearson theory [57]. This parameter evaluates the electronic flow in a reaction of two systems with different electronegativities, in particular case; a metallic surface (Fe) and an inhibitor molecule. ΔN is given as follows:

$$\Delta N = \frac{\chi_{Fe}-\chi_{inh}}{2(\eta_{Fe}+\eta_{inh})} \qquad (6)$$

Where χFe and χinh denote the absolute electronegativity of an iron atom (Fe) and the inhibitor molecule, respectively; ηFe and ηinh denote the absolute hardness of Fe atom and the inhibitor molecule, respectively. In order to apply the eq. 6 in the present study, a theoretical value for the electronegativity of bulk iron was used χFe = 7 eV and a global hardness of ηFe = 0, by assuming that for a metallic bulk I = A because they are softer than the neutral metallic atoms [57].
The electrophilicity has been introduced by Parr et al. [58], is a descriptor of reactivity that allows a quantitative classification of the global electrophilic nature of a compound within a relative scale. They have proposed the ω as a measure of energy lowering owing to maximal electron flow between donor and acceptor and ω is defined as follows.

$$\omega = \frac{\chi^2}{2\eta} \qquad (7)$$

The Softness σ is defined as the inverse of the η [59].

$$\sigma = \frac{1}{\eta} \qquad (8)$$

2.4. Molecular simulation study

The Metropolis Monte Carlo simulations (MCS) methodology [60] using the DMol3 module [61] and Adsorption Locator [62] implemented in the Materials Studio8.0 developed and distributed by BIOVIA (formerly Accelrys) [63], has been employed to build the system adsorbate/substrate.
The MCS process tries to find the lowest energy adsorption sites of the single inhibitor molecules on clean iron surface in water and hydrochloric acid solution system.
DMol3 geometry optimization was used to search the most stable conformational space of the single inhibitor molecule in the neutral form before putting it on the metallic surface and were performed by (m-GGA/ M11-L) functional [64] with the DNP+ as basis set for all atoms.
Simulations were carried out with a slab thickness of 5Å, a super cell of (7 × 7) and a vacuum of 30 Å along the Cz-axis in a simulation box (35,175 x 35,175 x 40,266 Å3) with periodic boundary conditions to model a representative part of the interface devoid of any arbitrary boundary effects.
For the whole simulation procedure, the Condensed-phase Optimized Molecular Potentials for Atomistic Simulation Studies (COMPASS) force field [65] is considered for calculating the interaction forces between different atoms; it was applied to find out the most adorable low energy adsorption sites along with their suitable configuration.
Finally, we can obtain the adsorption energy value for the most stable configuration of single inhibitor molecule (P1)/Fe (111)/10HCl/50H_2O system. Moreover, each adsorption system also included the effect of water and hydrochloric acid molecules to simulate the actual environment. More detail of Monte Carlo Method is referenced from the published article [66].

3. Results and discussion

3.1. Weightloss measurements

Mass loss studies were performed in the absence and presence of 1-benzyl-6-nitro-1H-indazole. The concentration in that molecule ranges from 10^{-6} to 10^{-3} M. The increase in 1-benzyl-6-nitro-1H-indazole concentration is accompanied by a decrease in corrosion rate and increase in inhibition efficiency (**Table 1**). These results show that 1-benzyl-6-nitro-1H-indazole P1 acts as an inhibitor of mild steel corrosion in 1M HCl.

3.2. Adsorption considerations

The adsorption isotherm reveals more information on the interaction between the metal surface and the inhibitor. Figure 3 shows the linear dependence of C/θ as a function of concentration C of inhibitors where θ is the surface coverage. The degree of surface coverage(θ) at different concentrations of the inhibitor in 1M HCl were evaluated from weight loss measures using the flowing formula:

$$\theta = E_W(\%)/100 \qquad (9)$$

Table 1. The weight loss parameters obtained for mild steel in 1 M HCl containing different concentrations of P1.

Inhibitor	Concentration (M)	*v* ($mg.cm^{-2} h^{-1}$)	E_w (%)	θ
1M HCl	--	0.828	--	--
P1	10^{-6}	0.289	65	0.65
	10^{-5}	0.213	74	0.74
	10^{-4}	0.125	85	0.85
	10^{-3}	0.078	91	0.91

Inhibitor adsorbs on the steel surface according to the Langmuir kind isotherm model which obeys the relation [67]:

$$\frac{C_{inh}}{\theta} = \frac{1}{K_{ads}} + C_{inh} \qquad (10)$$

$$K = \frac{1}{55.5} \exp\left(\frac{\Delta G^{\circ}}{RT}\right) \qquad (11)$$

K is the equilibrium constant of the adsorption process and 55.5 is the concentration of water in solution expressed in mol L^{-1}.

The Figure3 (plot of C/θ versus C) gives straight line with slope near to 1, meaning that the adsorption of the inhibitor under consideration on mild steel / acidic solution interface obeys Langmuir's adsorption.

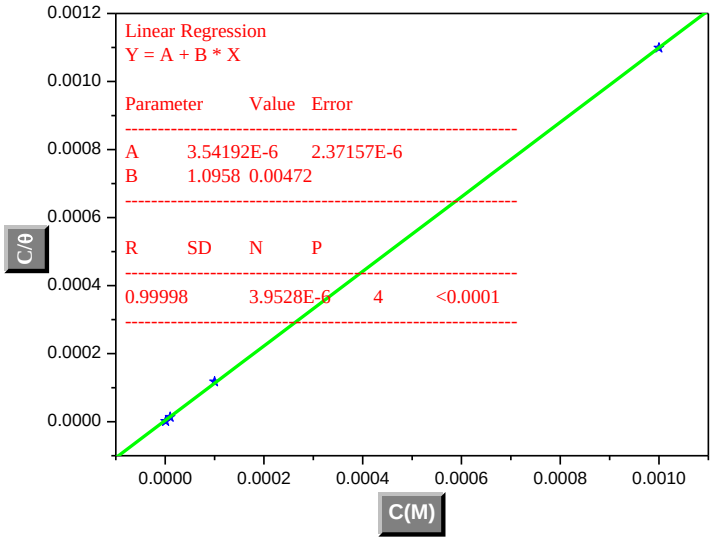

Figure 3: Langmuir adsorption of 1-benzyl-6-nitro-1H-indazole on the MS surface in 1M HCl solution at 308K.

The value of ΔG_{ads} for P1 is -40.10 kJ/mol. The large negative values of ΔGads confirmed the spontaneity of the adsorption process and stability of the adsorbed layer on the mild steel surface. Generally, the magnitude of ΔGads is around -20 kJ/mol or less negative is assumed to be due to electrostatic interaction between the inhibitor and the charged metal surface (i.e. physisorption). The values of ΔGads around -40 kJ/mol or more negative indicate that a charge sharing or transferring from organic species to the metal surface occurs to form a coordinate type of bond (i.e. chemisorption). The calculated values of ΔGads suggest a strong interaction between the inhibitor and the surface of mild steel, this interaction involves chemisorption [68].

3.3. Electrochemical impedance spectroscopy measurements

Nyquist impedance plots of MS in 1.0 M HCl solution containing different concentrations of 1-benzyl-6-nitro-1H-indazole (P1) are given in Figure 4. We can see that all impedance spectra display a single depressed capacitive arc over the frequency range studied, and this is often considered to related to the charge-transfer process [68]. The capacitive arcs are not perfect semicircles, and this difference could be attributed to the frequency dispersion as results of the roughness and inhomogeneous of electrode surface [69]. With the concentration of inhibitor increasing, the capacitive reactance arc radius became larger.

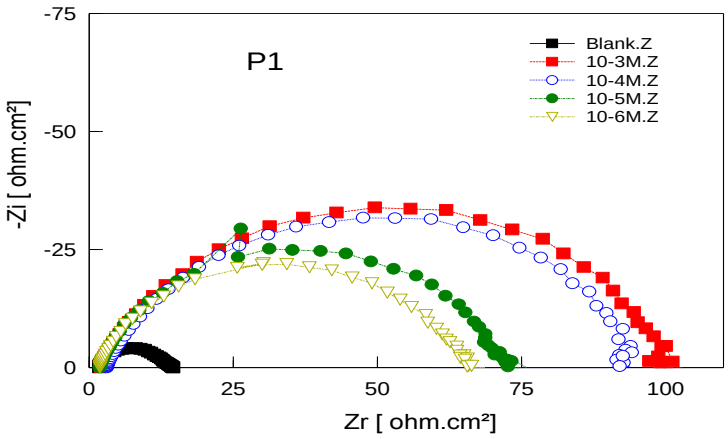

Figure 4. Nyquist plots for MS in 1.0 M HCl containing various concentrations of 1-benzyl-6-nitro-1H-indazole

The Randles equivalent circuit (Figure 5) model was used. *R*ct is the charge transfer resistance, *R*s is the solution resistance, and CPE represents a constant phase element. CPE has the value of the frequency-distributed double-layer capacitance. The impedance function of the CPE has the form [70].
The impedance function of the CPE has the form [70].

$$Z_{CPE} = \frac{1}{Y_0(j\omega)^n} \qquad (12)$$

Where*Y*0 is a proportionality coefficient, *j* is the imaginary number, $\omega$is the angular frequency ($\omega=2\pi f$, here *f* is the AC frequency in Hz), and *n* is a phase shift, which is related to the system homogeneity. When the CPE represents a pure capacitor, *n*=1. The capacitance values (*C*dl) can be calculated as follow:

$$C_{dl} = \frac{Y_0\omega^{n-1}}{\sin(n\pi/2)} \qquad (13)$$

The fitted impedance data such as *R*s, *R*ct and CPE constants *Y*0 and *n* are listed in Table 2.

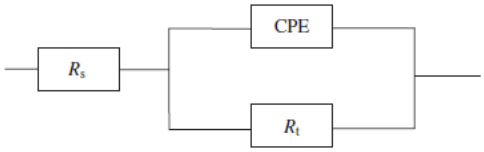

Figure 5. Equivalent circuit used to fit the EIS data.

As seen in Table 2, the R_{ct} values increased considerably after the addition of inhibitor, and they continuously increased as inhibitor concentration increases and hence an increase in inhibition efficiency. This can be attributed to the formation of an insulating layer on the mild steel surface, which forms a barrier for mass and charge-transfer at the electrode surface [68]. The thickness of the barrier layer (*d*) is related to *C*dl, *i.e.*, *C*dl=(ε0ε*S*)/*d*. Apparently the *C*dl values strongly decreased with increasing inhibitor concentration, which resulted from a decrease in the local dielectric constant $\varepsilon$and/or an increase in the thickness of the electrical

double layer, suggesting that the inhibitor strongly adsorbed to the metal/solution interface [68]. The best corrosion inhibition efficiency is 85% when the concentration of P1 is 10^{-3} M.

Table 2.EIS parameters obtained for mild steel in 1 M HCl in absence and presence of different concentration of P1 inhibitor.

Concentration (M) / Prameters	**1M HCl**	**10^{-6}**	**10^{-5}**	**10^{-4}**	**10^{-3}**
Real Center	9.25	33.739	37.114	48.21	51.02
Imag. Center	1.62	12.945	12.134	14.755	18.02
Diameter	15.13	69.288	74.821	94.502	104.19
n	0.81	0.84	0.86	0.83	0.82
Low Intercept R_s ($\Omega.cm^2$)	1.86	1.604	1.7261	3.3216	2.1388
High Intercept R_t ($\Omega.cm^2$)	16.64	65.874	72.502	93.098	99.901
Depression Angle	12.42	21.941	18.927	18.196	20.236
ω_{max} (rad s^{-1})	929.60	292.86	229.98	152.74	149.09
Estimated R_t($\Omega.cm^2$)	14.78	64.269	70.776	89.777	97.762
Estimated C_{dl}($F.cm^{-2}$)	7.11 E-5	6.9279E-5	6.4372E-5	5.8116E-5	4.9281E-5
E (%)	--	77	79	84	**85**

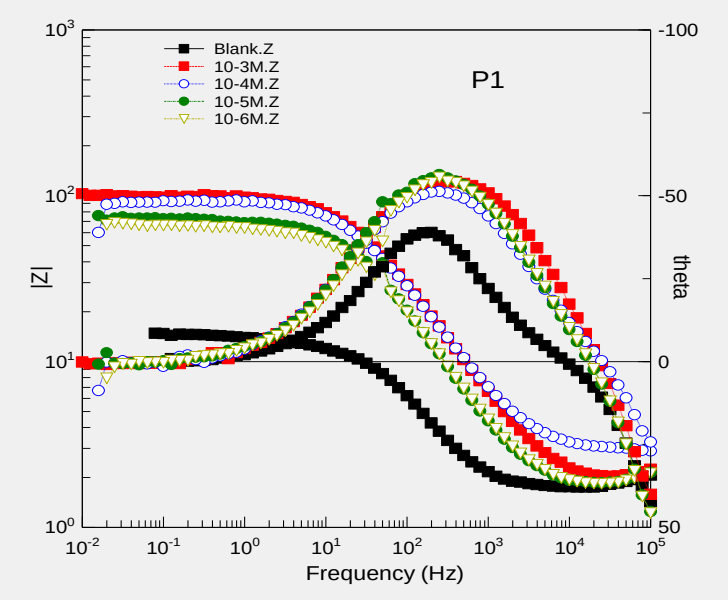

Figure 6. Bode plot for stainless steel in 1 M HCl solution containing various concentrations of inhibitors P1.

As seen from Figure 6, Bode plots refer to the existence of an equivalent circuit containing a single constant phase element in the interface of mild steel/solution. The increase of absolute impedance at low frequencies in Bode plot confirms the higher protection with the increasing of inhibitor P1 concentration. According to appearance of phase angle plots, increasing the concentration of P1 inhibitor in 1 M HCl results in more negative values of phase angle indicating good inhibitive behaviour of inhibitor which may be due to the adsorption of more inhibitor molecules on mild steel surface at higher concentration.

3.4. Potentiodynamic polarization measurements

Potentiodynamic polarization curves for mild steel in 1 M HCl without and with various concentrations of P1 at 308K are shown in Figure 7. The presence of P1 causes a prominent decrease in the corrosion rate i.e. shifts both anodic and cathodic curves to lower values of current densities. Namely, both cathodic and anodic reactions of mild steel electrode corrosion are drastically retarded by P1 in 1 M HCl.

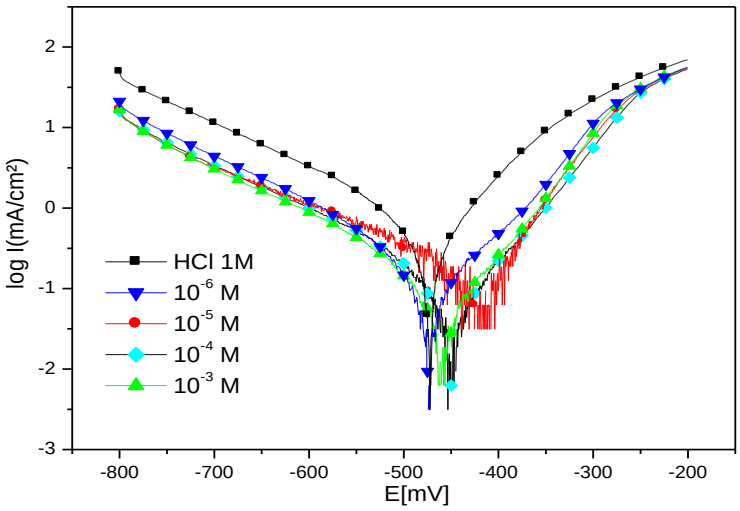

Figure 7. Potentiodynamic polarization curves for mild steel in 1 M HCl without and with different concentrations of P1 at 308K.

Values of corrosion current densities (I_{corr}), corrosion potential (E_{corr}), cathodic Tafel slope (βc), anodic Tafel slope (βa), and inhibition efficiency (Ep) are listed in Table 3. Clearly, Icorr decreases remarkably while Ep increases with the inhibitor concentration and the maximum Ep is up to 89% at 10^{-3}M P1. There is no definite trend in the shift of E_{corr} in the presence of P1, therefore, P1 can be arranged as a mixed-type inhibitor, and the inhibition action is caused by geometric blocking effect [68]. Namely, the inhibition action comes from the reduction of the reaction area on the surface of the corroding metal [70]. Tafel slopes of β_c and β_a do not change upon addition of P1, which indicates that adding P1 does not change the reaction mechanism.

Table 3. Potentiodynamic polarization parameters for the corrosion of mild steel in 1 M HCl containing different concentrations of P1 at 308K.

	C (M)	**E_{corr} (mV*vs.*SCE)**	**I_{corr} (μA/cm^2)**	**-βc (mV/dec)**	**βa (mV/dec)**	**E_p (%)**
1M HCl	--	-450	1381	140	185	--
P1	10^{-3}	-455	542	106	105	61
	10^{-4}	-444	410	133	110	70
	10^{-5}	-475	213	109	85	85
	10^{-6}	-467	151	94	75	**89**

Inhibition efficiencies obtained from weight loss (E_w), potentiodynamic polarization curves (E_p) and EIS are in good reasonably agreement.

3.5. Quantum chemical calculations

In the last few years, the FMOs (HOMO and LUMO) are widely used for describing chemical reactivity. The HOMO containing electrons, represents the ability (E_{HOMO}) to donate an electron, whereas, LUMO haven't not electrons, as an electron acceptor represents the ability (E_{LUMO}) to obtain an electron. The energy gap between HOMO and LUMO determines the kinetic stability, chemical reactivity, optical polarizability and chemical hardness–softness of a compound [71].

In this paper, we calculated the HOMO and LUMO orbital energies by using B3LYP method with 6-31G(d,p). All other calculations were performed using the results with some assumptions. The higher values of E_{HOMO} indicate an increase for the electron donor and this means a better inhibitory activity with increasing adsorption of the inhibitor on a metal surface, whereas E_{LUMO} indicates the ability to accept electron of the molecule. The adsorption ability of the inhibitor to the metal surface increases with increasing of E_{HOMO} and

decreasing of E_{LUMO}. High ionization energy (I= 6.67 eV, I= 3.46 eV in gas and aqueous phases respectively) indicates high stability [72-74], the number of electrons transferred (ΔN) was also calculated and tabulated in Table 4. The number of electrons transferred (ΔN) was also calculated and tabulated in Table 5. The ΔN(gas) < 3.6 and ΔN(aqueous) < 3.6 indicates the tendency of a molecule to donate electrons to the metal surface [75].

Table 4. Quantum chemical descriptors of the studied inhibitor at B3LYP/6-31G(d,p) in gas, G and aqueous, A phases

Prameters	Phase	
	Gas	Aqueous
Total Energy *TE* (eV)	-23693.1	-23693.5
E_{HOMO} (eV)	-3.6105	-6.7198
E_{LUMO} (eV)	-1.5382	-1.5178
Gap ΔE (eV)	2.0723	5.2020
Dipole moment μ (Debye)	3.2235	3.7417
Ionisation potential I (eV)	3.6105	6.7198
Electron affinity A	1.5382	1.5178
Electronegativity χ	2.5743	4.1188
Hardness η	1.0362	2.6010
Electrophilicity index ω	3.1980	3.2611
Softness σ	0.9651	0.3845
Fractions of electron transferred ΔN	2.1356	0.5539

The calculated values of the f_k^+ for all inhibitors are mostly localized on the indazole ring. Namely C_3, N_{11}, O_{12}, O_{13}, C_{24},N_{28} and N_{29}, indicating that the indazole ring will probably be the favorite site for nucleophilic attacks. The results also show that O_{14} atom is suitable site to undergo both nucleophilic and electrophilic attacks, probably allowing them to adsorb easily and strongly on the mild steel surface.

Table5. Pertinent natural populations and Fukui functions of the studied inhibitors calculated at B3LYP/6-31G(d,p) in gas, G and aqueous, A phases.

Atom k	*phase*	*P(N)*	*P(N-1)*	*P(N+1)*	f_k^-	f_k^+	f_k^0
C_3	*G*	6,22279	6,35169	6,14786	0,1289	0,0749	0,1019
	A	6,21788	6,33946	6,15457	0,1216	0,0633	0,0924
N_{11}	*G*	6,51139	6,59527	6,49592	0,0839	0,0155	0,0497
	A	6,47721	6,6126	6,47084	0,1354	0,0064	0,0709
O_{12}	*G*	8,37564	8,54389	8,33335	0,1682	0,0423	0,1053
	A	8,39704	8,5907	8,37152	0,1937	0,0255	0,1096
O_{13}	*G*	8,38492	8,54636	8,35235	0,1614	0,0326	0,0970
	A	8,40172	8,59326	8,37844	0,1915	0,0233	0,1074
C24	*G*	6,22992	6,2503	6,14648	0,0204	0,0834	0,0519
	A	6,23802	6,24601	6,12189	0,0080	0,1161	0,0621
N_{28}	*G*	7,01569	7,12076	6,99647	0,1051	0,0192	0,0621
	A	7,03173	7,11136	6,99425	0,0796	0,0375	0,0586
N_{29}	*G*	7,24158	7,27952	7,13087	0,0379	0,1107	0,0743
	A	7,26838	7,29555	7,16869	0,0272	0,0997	0,0634

The final optimized geometries of P1 in gas and aqueous, selected valence bond angle and dihedral angles and bond lengths are given in Figure8.

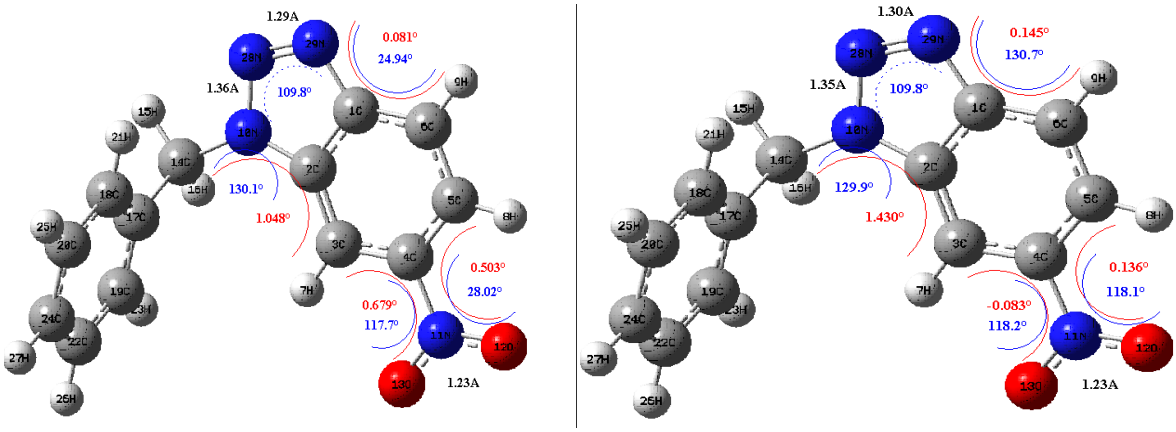

P1Gas phase **P1** Aqueous phase

Figure 8. Optimized molecular structures, selected dihedral angles (red), valence bond angle (blue) and bond lengths (black) of the studied inhibitors calculated in gas and aqueous phases at B3LYP/6-31G(d,p) levelof **P1**

After the analysis of the theoretical results obtained, we can say that the molecule**P1** have a non-planar structure.

Table 6 : The HOMO and the LUMO electrons density distributions of the studied inhibitors computed at B3LYP/6-31G (d,p) level in gas and aqueous phases.

	P1Gas phase	**P1**Aqueous phase
HOMO	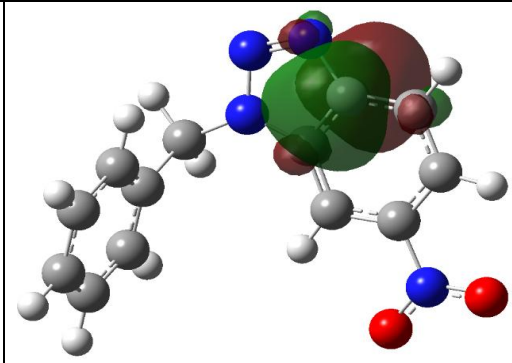	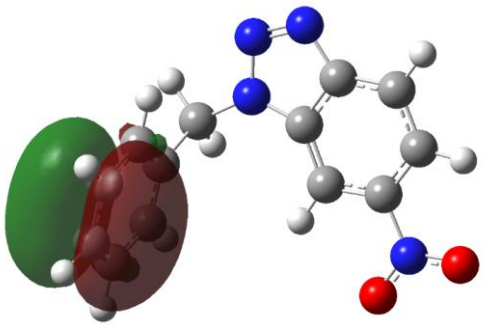
LUMO	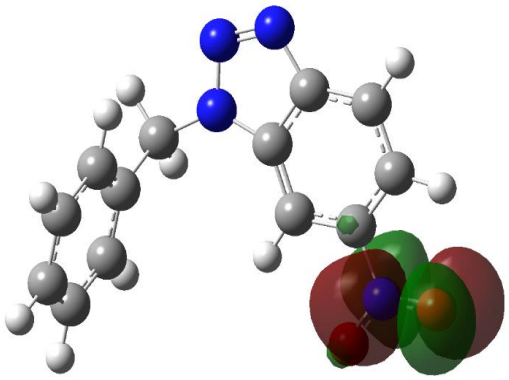	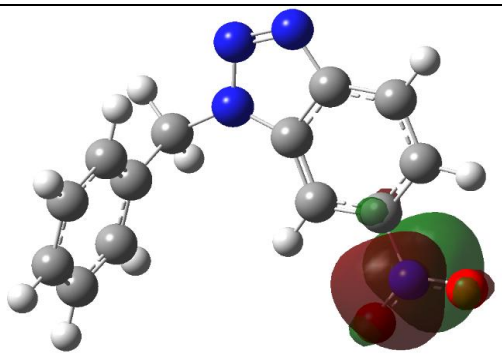

The inhibition efficiency afforded by P1 may be attributed to the presence of electron rich O.

3.6. Molecular simulation study

In the current study, the studied inhibitor molecule (P1) has been simulated as adsorbate on steel surface (111) substrate in presence of some molecules of water and hydrochloric acid to find the most favorable configuration

for single inhibitor molecule (P1), solvent molecules and steel surface system as the temperature is slowly decreased. Molecular dynamics techniques are applied on a system comprising a (one-inhibitor molecule (P1) /50H_2O/10HCl / Fe (111)). Each inhibitor molecule (P1) is placed on the iron surface (111), optimized and then run quench molecular dynamics. The Monte Carlo simulation process tries to find the lowest energy for the whole system. The structure of the adsorbate (P1) is minimized until it satisfies certain specified criteria. The optimization energy curve of single inhibitor molecule (P1) in the neutral form before putting it on Fe (111) surface obtained by $DMol^3$ module at m-GGA/ M11-L /DNP+ level has been presented in Figure 9.

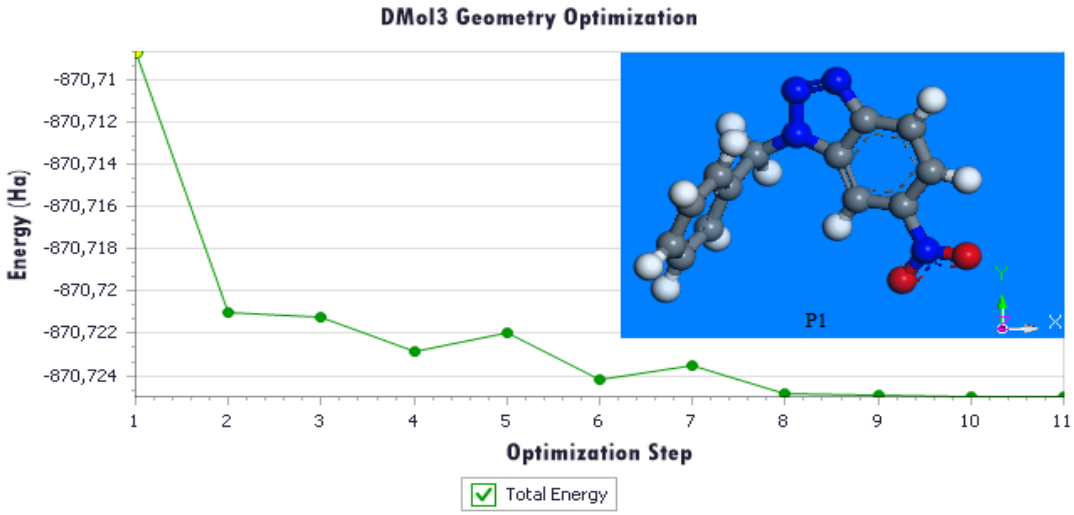

Figure 9. Optimized geometric structure for the neutral form of P1-inhibitor in aqueous phase at m-GGA/ M11-L/DNP+ level of theory.

The Metropolis Monte Carlo method in Adsorption Locator module provides four step types for a canonical ensemble: conformer, rotation, translation and regrowth [76]. The adsorption energy distribution for (Fe (111) / P1 / 50 H_2O/10HCl) system obtained by adsorption locator module are shown in **Figure10**.

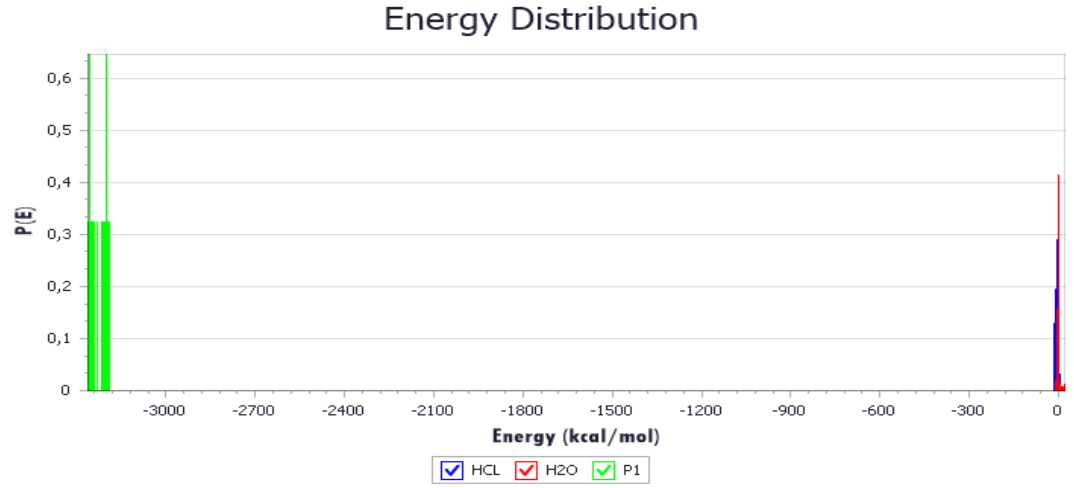

Figure 10. Energy distribution for Fe (111) / P1 /50H_2O/10HCl interface obtained through the Monte Carlo simulation.

Figure 10 shows the adsorption energy distribution of inhibitor molecule (P1) on steel surface in water and hydrochloric acid solution. The adsorption energy of inhibitor molecule (P1) reaches (-118,06Kcal/ mol), which shows the adsorption stronger for Fe-inhibitor (P1) complex.
A typical adsorption energy distribution of Fe (111) / P1 /50H_2O/50HCl system consisting of total energy, Van der Waals energy, average total energy, electrostatic energy and intermolecular energy is given in Figure 11.
Figure 11 shows total energy distribution for Fe (111) / (P1) / 50 H_2O/10HCl system during energy optimization process. The equilibrium configurations of the single inhibitor molecule (P1) adsorbed onto the iron surface (111) in water and hydrochloric acid molecules obtained by adsorption locator module are given in Figure 12.

Side and top views of the most suitable P1 conformation adsorbed on the Fe (111)/50 H_2O/10HCl interface obtained through the Monte Carlo simulation as shown in Figure12.

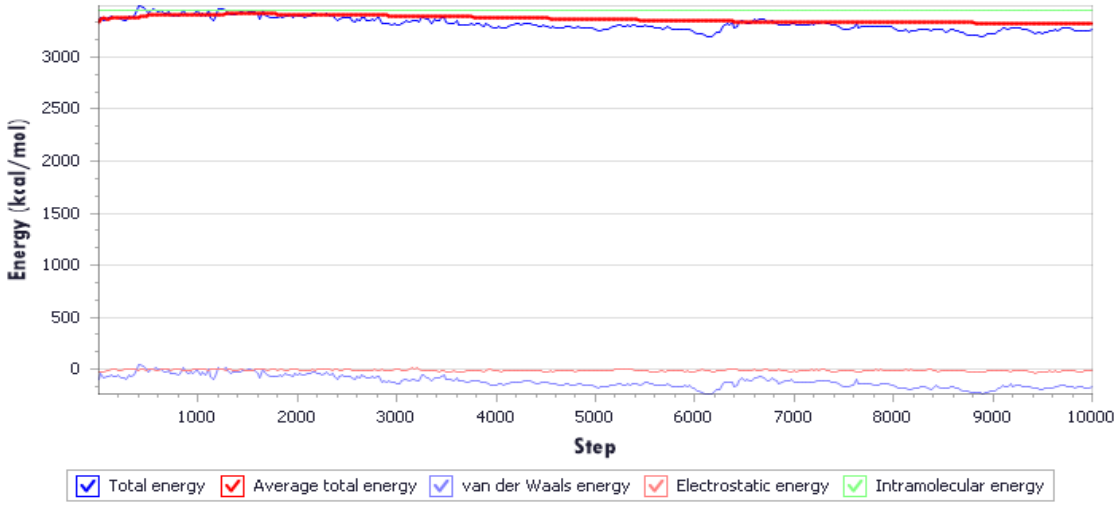

Figure 11. Total energy distribution for Fe (111) / (P1) / 50 H_2O/10HCl complex during energy optimization process calculated by adsorption locator module.

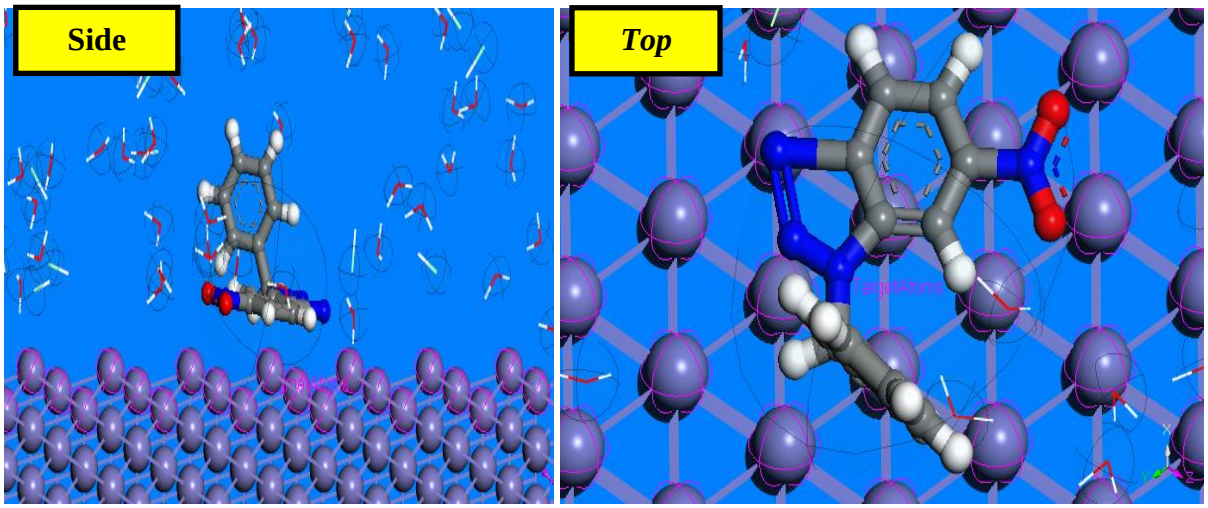

Figure 12. Side and top views of most stable adsorption configuration for Fe (111) / P1 / 50 H_2O/10HCl interface obtained through the Monte Carlo simulation.

As seen in Figure 12, it can be observed that the adsorption actives centers on the iron surface (111) are the lone pair of electrons on the atoms(=N- &-O-) and Π-electrons of nitro-indazole ring and observed also that the neutral form of inhibitor molecule (P1) adsorbed in a planar manner onto the Fe (111) in acid medium, to maximize contact and surface coverage, ensuring a strong interaction for Fe (111) / P1 /50 H_2O/10HCl interface. This is mainly due to the extension of a high inhibition effect observed experimentally (IE_{exp} tend to 91%). For the Fe-inhibitor (P1) complex, the calculated dihedral angles around the nitro-indazole ring are close to 0° or 180°, indicating planarity of the nitro-indazole ring.

Noteworthy, the bond angles between Fe, (-O- or –N=) and (=C-) of nitro-indazole ring after molecular adsorption on iron surface(111) is: $\alpha_{Fe\text{-}O13\text{-}N12}$:+83.364°, $\alpha_{Fe\text{-}O14\text{-}C12}$:+131.78°, $\alpha_{Fe\text{-}N11\text{-}C2}$:+104,617°and $\alpha_{Fe\text{-}N30\text{-}N10}$:+135,160°, which indicate that the 1-benzyl-6-nitro-1H-indazole are nearly parallel onto the iron surface (111) in aqueous acid solution.

The measured shortest bond distances (**Fig12**) between the closest heteroatoms (-O- & =N-) of nitro-indazole ring and iron surface (111) at equilibrium were as follows: Fe-inhibitor (P1) complex: ($d_{Fe–O13}$: 3.55Å, $d_{Fe–O14}$: 2.747Å, $d_{Fe–N10}$: 3.399Å, $d_{Fe–N30}$: 3.094Å and $d_{Fe–N11}$: 2.921Å),it is observed from the bond distances, that all the

bond distances exist at around 2.7-3.55Å, which signifies that the chemical bonds can be formed between active centers(-O_{13}-,-O_{14}-,=N_{10}-,=N_{30}-&=N_{11}-) of investigated compound and Fe(111) atoms, confirming the high inhibition efficiency of tested inhibitor [77]**.**
The outputs and descriptors calculated by the Monte Carlo simulation of P1 conformations on iron (111) surface in water and hydrochloric acid solution obtained through the Monte Carlo simulation, such as total energy, adsorption energy, rigid adsorption energy and deformation energy are exposed in **Table 7.**

Table 7. Outputs and descriptors for the lowest adsorption configurations for Fe (111) / P1/ 50 H_2O/10HCl interface obtained through the Monte Carlo simulation. (All values in Kcal/mol).

structures	E_T	E_A 10^{+3}	R.A.E	D_E 10+	dE_{ads}/dN_i P1*10^3	dE_{ads}/dN_i HCl	dE_{ads}/dN_i H_2O
Substrate	0,000						
P1	3,98*10^3						
HCl	1,694						
H_2O	0,0303						
Fe (1 1 1) - 1	-875,608	-4,916	-911,67	-4,005	-4,066	-16,052	-9,341
Fe (1 1 1) - 2	-858,808	-4,899	-895,53	-4,004	-4,063	-16,454	-8,340
Fe (1 1 1) - 3	-848,491	-4,889	-884,32	-4,005	-4,057	-15,836	-7,586
Fe (1 1 1) - 4	-845,939	-4,887	-882,85	-4,004	-4,063	-15,964	-7,351
Fe (1 1 1) - 5	-841,168	-4,882	-876,26	-4,006	-4,060	-15,872	-0,833
Fe (1 1 1) - 6	-832,529	-4,873	-868,58	-4,005	-4,061	-16,015	-0,395
Fe (1 1 1) - 7	-831,830	-4,872	-867,59	-4,005	-4,062	-15,902	-0,143
Fe (1 1 1) - 8	-826,306	-4,867	-860,22	-4,007	-4,056	-16,330	-6,101
Fe (1 1 1) - 9	-823,424	-4,864	-856,53	-4,008	-4,060	-16,247	-0,543
Fe (1 1 1) - 10	-823,070	-4,864	-857,96	-4,006	-4,062	-16,184	-0,273

The parameters presented in **Table 7** include total energy (E_T), in Kcal/mole, of the substrate/adsorbate system. The total energy is defined as the sum of adsorption energy and the internal energy of the sorbate [11]**.** In addition, the adsorption energy (E_A) for the Fe (111) / P1 / 10HCl/50 H_2O interface obtained by the Monte Carlo simulation were calculated. The adsorption energy is given by the formula as:

$$E_A = E_{(P1/50HCl/50H2O/Fe(111)} - (E_{P1} - E_{Fe(111)} - E_{50H2O} - E_{50HCl}) \qquad (14)$$

The adsorption energy is defined as the sum of the rigid adsorption energy (R.A.E) and the deformation energy (D_E) for the adsorbate components. The rigid adsorption energy reports the energy, in Kcal/mol, released (or required) when the unrelaxed P1 molecule, before the geometry optimization step are adsorbed on the iron surface (111) in acid medium. The deformation energy (D_E) reports the energy, in Kcal/mol, released when the adsorbed inhibitor molecule (P1) is relaxed on the iron surface (111). Table 7 also gives (dE_A/dN_i), which reports the energy of substrate–adsorbate configuration where one of adsorbate component has been removed.
It is quite clear from Table 7 that all adsorption energy values for Fe (111)/P1/50H_2O/10HCl) system is negative, which suggest that the inhibitor molecule (P1) is quickly and tightly adsorbed onto the iron surface (111) in acid solution. High absolute value of the adsorption energy reflects a strong adsorption behavior [78]. The adsorption energy value of the P1 (-4,91610^{3}Kcal/mol) in equilibrium configuration, is far higher than that of water molecules (-9,341Kcal/mol) and hydrochloric acid molecules (-16,052Kcal/mol). This indicates the possibility of a progressive replacement of the water and hydrochloric acid molecules from the surface of the iron leading to the formation of a stable layer that can protect the plate against aqueous corrosion. The result indicate that the inhibitor molecule (P1) has the strongest interaction with the iron surface(111) in water and Hydrochloric acid solution, which corroborate very well with inhibition efficiency obtained from experimental results. The adsorption density of inhibitor molecule (P1) on the metal surface in water and Hydrochloric acid solution are given in **Fig 13**.
As can be seen from Figure 5, the inhibitor molecule (P1) is likely to adsorb on the iron surface (111) in acid medium to form stable organic adsorption layers, and can be seen as a barrier to protect iron from corrosion. In addition, it has high adsorption energy to Fe surface as seen in Table 7.

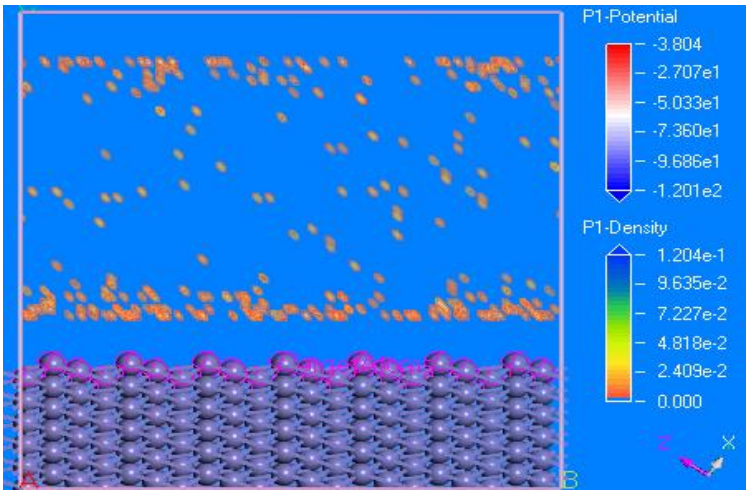

Figure13. Adsorption density field for Fe (111) / P1/ 50HCl/50 H_2O interface obtained through the Monte Carlo simulation.

Conclusion

The following conclusions may be drawn from the study:

- The inhibition efficiency of indazole derivative (P1) for mild steel in HCl solution increases with increasing concentration.
- The corrosion current density significantly decreases and corrosion potential slightly changes with the addition of P1 in HCl solution, and the synthesized inhibitor of P1 is mixed type inhibitor.
- The adsorption of P1 on the mild steel surface obeys Langmuir isotherm.
- The presence of P1 in 1.0 M HCl solution increases charge transfer resistance, while it reduces double layer capacitance values. This result can be attributed to the increase of electrical double layer's thickness.
- The large efficiency of an inhibitor P1 is due to the presence of many atom of oxygen in this indazole derivative. The calculated quantum chemical parameters such as HOMO-LUMO gap, E_{HOMO}, E_{LUMO}, dipole moment (μ) and total energy (TE) were found to give reasonably good correlation with the efficiency of the corrosion inhibition.
- Both experimental, quantum chemical and Monte Carlo simulations results showed that the inhibition efficiency of P1 is affected by the heteroatoms (N,O) and π-system presented in our compound.

References

1. Elmsellem H., Youssouf M. H., Aouniti A., Ben Hadd T., Chetouani A., Hammouti B. *Russian, Journal of Applied Chemistry*. 87 (2014) 744−753.
2. Hjouji M. Y., Djedid M., Elmsellem H., Kandri Rodi Y., Benalia M., Steli H., Ouzidan Y., Ouazzani Chahdi F., Essassi E. M., and Hammouti B. *Der Pharma Chemica*. 8 (2016)85-95.
3. Elmsellem H., Harit T., Aouniti A., Malek F., Riahi A., Chetouani A., and Hammouti B., *Protection of Metals and Physical Chemistry of Surfaces*. 51 (2015) 873–884.
4. Bentiss F., Lagrenee M., Traisnel M., Hornez J.C., *Corros. Sci*. 41(1999) 789.
5. Essaghouani A. L., Elmsellem H., Ellouz M., El Hafi M., Boulhaoua M., Sebbar N. K., Essassi E. M., Bouabdellaoui M., Aouniti A. and Hammouti B., *Der Pharma Chemica*. 8(2) (2016)297-305.
6. Ellouz M., Elmsellem H., Sebbar N. K., Steli H., Al Mamari K., Nadeem A., Ouzidan Y., Essassi E. M., Abdel-Rahaman I., Hristov P., *J. Mater. Environ. Sci*. 7(7) (2016)2482-2497.
7. Elmsellem H., Bendaha H., Aouniti A., Chetouani A., Mimouni M., Bouyanzer A., *Mor. J. Chem*. 2 (2014) 1.
8. Elmsellem H., Elyoussfi A., Sebbar N. K., Dafali A., Cherrak K., Steli H., Essassi E. M., Aouniti A. and Hammouti B., *Maghr. J. Pure & Appl. Sci*. 1 (2015)1-10.
9. Elmsellem H., Karrouchi K., Aouniti A., Hammouti B., Radi S., Taoufik J., Ansar M., Dahmani M., Steli H., El Mahi B., *Der Pharma Chemica*, 7 (2015)237-245.
10. Elmsellem H., Elyoussfi A., Steli H., Sebbar N. K., Essassi E. M., Dahmani M., El Ouadi Y., Aouniti A., El Mahi B., Hammouti B., *Der Pharma Chemica*. 8(1) (2016) 248.

11. Elmsellem H., Basbas N., Chetouani A., Aouniti A., Radi S., Messali M., Hammouti B., *Portugaliae. Electrochimica. Acta*. 2 (2014) 77.
12. Elmsellem H., Nacer H., Halaimia F., Aouniti A., Lakehal I., Chetouani A., Al-Deyab S. S., Warad I., Touzani R., Hammouti B, *Int. J. Electrochem. Sci*. 9 (2014) 5328.
13. Elmsellem H., Aouniti A., Youssoufi M.H., Bendaha H., Ben hadda T., Chetouani A., Warad I., Hammouti B., *Phys. Chem. News*. 70 (2013) 84.
14. Tribak Z., Kandri Rodi Y., Elmsellem H., Abdel-Rahman I., Haoudi A., Skalli M. K., Kadmi Y., Hammouti B., Ali Shariati M., Essassi E. M., *J. Mater. Environ. Sci*. 8 (2017) 1116 -1127
15. Elmsellem H., Aouniti A., Toubi Y., Steli H., Elazzouzi M., Radi S., Elmahi B., El Ouadi Y., Chetouani A., Hammouti B., *Der Pharma Chemica*. 7 (2015) 353-364.
16. Elmsellem H., Aouniti A., Khoutoul M., Chetouani A., Hammouti B., Benchat N., Touzani R., Elazzouzi M., *J. Chem. Pharm. Res.* 6(2014)1216.
17. Sikine M., Kandri Rodi Y., Elmsellem H., Krim O., Steli H., Ouzidan Y., Kandri Rodi A., Ouazzani Chahdi F., Sebbar N. K., Essassi E. M., *J. Mater. Environ. Sci*. 7 (4) (2016) 1386-1395.
18. Hjouji M. Y., Djedid M., Elmsellem H., Kandri Rodi Y., Ouzidan Y., Ouazzani Chahdi F., Sebbar N. K., Essassi E. M., Abdel-Rahman I., Hammouti B., *J. Mater. Environ. Sci.* 7 (4) (2016) 1425-1435
19. Bendaha H., Elmsellem H., Aouniti A., Mimouni M., Chetouani A., Hammouti B., *Physicochemical Mechanics of Materials.* 1 (2016) 111-118.
20. Quraishi M.A., Sharma H.K., *Chem. Phys*. 78 (2002) 18.
21. Quraishi M.A., SardarR., *Mater. Chem. Phys*. 78 (2002) 425.
22. Bentiss F., Gassama F., Barbry D., Gengembre L., Vezin H., Lagrene´e M., Traisnel M., *Appl. Surf. Sci.* 252 (2006) 2 684.
23. Khaled K.F., Hackerma N., *Electrochim. Acta*. 48 (2003) 2715.
24. Zarrouk A., Zarrok H., Salghi R., Hammouti B., Al-Deyab S.S., Touzani R., Bouachrine M., Warad I.,Hadda T. B., *Int. J. Electrochem. Sci*.7 (2012) 6353 – 6364.
25. Verma C., Ebenso E., Bahadur I., Obot I., Quraishi M., *J. Mol. Liq*. 212 (2015) 209–218.
26. Bentiss F., Jama C., Mernari B., El Attari H., El Kadi L., Lebrini M., Traisnel M., Lagrenée M., *Corros. Sci*. 51 (2009) 1628.
27. Lahmidi S., Elyoussfi A., Dafali A., Elmsellem H., Sebbar N. K., El Ouasif L., E. Jilalat A., El Mahi B., Essassi E. M., Abdel-Rahman I., Hammouti B., *J. Mater. Environ. Sci.* 8 (1) (2017) 225-237.
28. Sikine M., Elmsellem H., Kandri Rodi Y., Steli H., Aouniti A., Hammouti B., Ouzidan Y., Ouazzani Chahdi F., Bourass M., Essassi E.M., *J. Mater. Environ. Sci.* 7 (12) (2016) 4620-4632.
29. Atta-us-Rahman M. S., He C. H.,Clardy J., *Tetrahedron. Lett.* 26 (1985) 2759.
30. Liu Y. M., Yang J. S., Liu Q. H., *Chem. Pharm. Bull*.52 (2004) 454.
31. Ali Z., Ferreira D., Carvalho P., Avery M. A., Khan I. A., *J. Nat. Prod*. 71 (2008) 1111.
32. Cerecetto H., Gerpe A., Gonzalez M., Aran V. J., de Ocariz C. O., *Med. Chem*. 5 (2005) 869.
34. Watson T. J., Ayers T. A., Shah N., Wenstrup D., Webster M., Freund D., Horgan S., CareyJ. P., *Org. Process Res. Dev*. 7 (2003) 521.
35. Caron S.,Vazquez E., *Synthesis*. 4 (1999) 588.
36. Yeu J.P., Yeh J.T., Chen T.Y., Uang B.J., *Synthesis*. 1775 (2001) 30.
37. Speranza M., *Adv. Heterocycl. Chem*. 40 (1985)25.
38. Bouillon I., Zajicek J., Pudelova N., Krchnak V., *J. Org. Chem*. 73 (2008) 9027.
39. Campetella S., Palmieri A., Petrini M., *Eur. J. Org. Chem*. 19 (2009) 3184.
40. Kylmala T., Udd S., Tois J., Franzen R., *Tetrahedron Lett*. 51 (2010) 3613.
41. Spiteri C., Keeling S., Moses J., *E. Org. Lett*. 12 (2010) 3368.
42. Counceller C. M., Eichman C. C., Wray B. C., Stambuli J., *P. Org. Lett*. 10 (2008) 1021.
43. Chakib I., Elmsellem H., Sebbar N. K., Lahmidi S., Nadeem A., Essassi E. M., Ouzidan Y., Abdel-Rahman I., Bentiss F., Hammouti B., *J. Mater. Environ. Sci*. 7(6) (2016)1866-1881.
44. Frisch M.J., Trucks G.W., Schlegeletal H.B.., *Gaussian 09, Revision A.1, Gaussian, Inc.,Wallingford, Conn, USA*, (2009).
45. Tribak Z., Kandri Rodi Y., Elmsellem H., Abdel-Rahman I., Haoudi A., Skalli M. K., Kadmi Y., Hammouti B., Ali Shariati M., Essassi E. M.,*J. Mater. Environ. Sci*., 8 (3) (2017)1116-1127.
46. Li J., Li H., Jakobsson M., Li S., Sjodin P., Lascoux M., *Mol. Ecol.*21(1) (2012) 28-44.

47. Elyoussfi A., Dafali A., Elmsellem H., Steli H., Bouzian Y., Cherrak K., El Ouadi Y., Zarrouk A., HammoutiB., *J. Mater. Environ. Sci.* 7 (9) (2016) 3344.
48. Zarrouk A., Hammouti B., Zarrok H., Bouachrine M., Khaled K.F., Al-Deyab S.S., *Int. J. Electrochem. Sci*. 6 (2012) 89.
49. Efil K., Bekdemir Y. *Canadian Chemical Transactions*. 3(1) (2015) 85.
50. Pauling L., The nature of the chemical bond, 3rd edn. (Cornell University Press, Ithaca,) (1960).
51. Sen, K. D., Jorgenson, C. K. Eds. Structure and Bonding, Electronegativity, Springer: Berlin, 66 (1987).
52. Sen K.D., Mingos D.M.P. (eds.), in Chemical Hardness, Structure and Bonding, Springer-Verlag, Berlin, 80 (1993) 11–25.
53. Parr R. G., Yang W., Density-Functional Theory of Atoms and Molecules. Oxford University Press, New York, (1989).
54. Geerlings P., de Proft F., Langenaeker W., *Chem. Rev*. 103 (2003) 1793.
55. Chermette H., *J. Comput. Chem*. 20 (1999)129.
56. Roy R.K., Pal S., Hirao K., *J. Chem. Phys*. 110(1999) 8236.
57. Pearson R.G., *Inorg. Chem*., 27 (1988) 734.
58. Sastri, V.S. and Perumareddi, J.R., *Corrosion*.3 (1997) 671.
59. Udhayakala P., Rajendiran T. V., Gunasekaran S., *Journal of Chemical, Biological and Physical Sciences* A, 2(3) (2012)1151–1165.
60. Metropolis N., Rosenbluth AW., Rosenbluth MN., Teller AH., Teller E., J. Chem. Phys., 21 (1953) 1087.
61. Delley B., J. Chem. Phys., 113 (2000) 7756.
62. Frenkel D., Smit B., Understanding Molecular Simulation: From Algorithms to Applications, 2nd Edition, Academic Press, San Diego (2002).
63. Biovia Materials Studio version 8.0, Accelrys Inc. USA., (2014).
64. Xiong R., Sandler S. I., Burnett R. I., *Ind. Eng. Chem. Res*. 53 (2014)8265-8278.
65. Belghiti ME., Karzazi Y., Dafali A., Obot I.B., Ebenso EE., Emrane KM., Bahadur I., Hammouti B., Bentiss F., *J. Mol. Liq.*, 216 (2016) 874-886.
66. Karzazi Y., Belghiti M. E., El-Hajjaji F. and Hammouti B., *J. Mater. Environ. Sci*. 7 (10) (2016) 3916.
67. Zarrok H., Zarrouk A., Salghi, R., Oudda H., Hammouti B., Assouag M., Taleb M., Ebn Touhami M., Bouachrine M., Boukhris S., *J. Chem. Pharm. Res.* 4 (2012) 5056.
68. Elmsellem H., Youssouf M. H., Aouniti A., Ben Hadd T., Chetouani A., Hammouti B.. *Russian, Journal of Applied Chemistry*, 87(6)(2014) 744−753.
69. Aouniti A., Elmsellem H., Tighadouini S., Elazzouzi M., Radi S., Chetouani A., Hammouti B., Zarrouk A., *J. Taibah Univ. Sci*. 10 (2016) 774-785.
70. Sebbar N.K., Elmsellem H., Boudalia M., lahmidi S., Belleaouchou A., Guenbour A., Essassi E.M., Steli H,. Aouniti A. *J. Mater. Environ. Sci.* 6 (11) (2015) 3044
71. Govindarajan M., Karabacak M., *Spectrochim Acta Part A Mol Biomol Spectrosc*. 85(2012) 251–260.
72. Ramdani M., Elmsellem H., Elkhiati N., Haloui B., Aouniti A., Ramdani M., Ghazi Z., Chetouani A. and Hammouti B., *Der pharma chem.*7 (2015) 67-76.
73. Hjouji M. Y., Djedid M., Elmsellem H., Kandri Rodi Y., Ouzidan Y., Ouazzani Chahdi F., Sebbar N. K., Essassi E. M., Abdel-Rahman I., Hammouti B., *J. Mater. Environ. Sci*, 7 (4) (2016) 1425-1435.
74. Ellouz M., Elmsellem H., Sebbar N. K., Steli H., Al Mamari K., Nadeem A., Ouzidan Y., Essassi E. M., Abdel-Rahaman I., Hristov P., *J. Mater. Environ. Sci*. 7(7) (2016) 2482-2497.
75. Lukovits I., Kalman E., Zucchi F., *Corrosion*, 57 (2001) 3-7.
76. Guedes Soares C., Garbatov Y., Zayed A., Wang G., *Corros. Sci*. 50 (2008) 3095.
77. Abdel-Gaber A.M., Abd-El-Nabey B.A., Sidahmed I.M., El-Zayady A.M., Saadawy M., *Corros. Sci*. 48 (2006) 2765–2779.
78. Guo L., Zhu S., Zhang S., He Q. & Li W., *Corros. Sci*. 87 (2014) 366–375.